

From:
Atom Interferometry
Paul R. Berman (ed.)
Academic Press, San Diego,
1997.

ATOM INTERFEROMETRY BASED ON SEPARATED LIGHT FIELDS

UWE STERR, KLAUS SENGSTOCK, WOLFGANG ERTMER
Institut für Quantenoptik, Universität Hannover, Hannover, Germany

FRITZ RIEHLE, JÜRGEN HELMCKE
Physikalisch-Technische Bundesanstalt, Braunschweig, Germany

| | |
|--|-----|
| I. Introduction | 293 |
| II. Theoretical Framework | 299 |
| A. The Four-Beam Bordé Interferometer | 300 |
| B. Pulsed Interferometer | 302 |
| C. General Description | 304 |
| III. Discussion of Different Types of Interferometers | 312 |
| IV. Experimental Realization of Bordé Interferometry | 318 |
| A. Interferometry on a Thermal Atomic Beam | 320 |
| B. Interferometry on a Laser Cooled Atomic Beam | 322 |
| C. Interferometry on Trapped Atoms | 324 |
| D. Discussion of Experimental Parameters | 326 |
| E. Suppression of One Recoil Component | 329 |
| V. Precision Determination of Physical Quantities | 331 |
| A. Measurements of dc Stark Shift and Atomic Polarizabilities | 331 |
| B. Phase Shifts by the ac Stark Effect | 335 |
| C. Determination of the Dipole Moment of a Weak Transition | 337 |
| VI. Geometrical and Topological Phases | 339 |
| A. Measurement of the Scalar Aharonov–Bohm Effect | 340 |
| B. Measurement of the Aharonov–Casher Effect | 343 |
| C. Measurement of the Sagnac Effect | 346 |
| VII. Influence of the Quantum-Mechanical Measurement Process in the Interferometer | 349 |
| VIII. Applications of Atom Interferometry in Optical Frequency Standards | 351 |
| A. Atom Interference as a Discriminator for Frequency Stabilization | 352 |
| B. Optical Frequency Measurement | 354 |
| C. Frequency Uncertainty of the Optical Frequency Standard | 355 |
| IX. Conclusions | 358 |
| References | 358 |

I. Introduction

The recent development in atom interferometry has greatly stimulated new fields in atomic physics and quantum optics, opening up new areas in fundamental and applied research. Atom interferometry offers interesting possibilities for carrying out fundamental research in such fields as quantum optics and atom optics;

In parallel with a better understanding of this type of atom interferometer, ideas and experiments for generalized interferometers (Bordé, 1992) have been developed. Extended and specialized interferometer geometries include, for example, the use of crossover resonances (Dingler *et al.*, 1994), copropagating laser waves (Morinaga and Ohuchi, 1995), and multiple laser beam setups (Morinaga, 1992). We will discuss these interferometers in Section III.

A further important step was the use of laser cooled atoms as source for the interferometer, allowing one to vary the de Broglie wavelength in a large range and increase the sensitivity for a certain class of experiments. Witte *et al.* (1992) used a laser decelerated and deflected atomic Ca beam. A different class of experiments uses laser stored atoms nearly at rest in space and pulsed excitation (Sengstock *et al.*, 1993a, Kisters *et al.*, 1994). This leads as a new concept to interference in the time domain, which offers several advantages compared with interference in the spatial domain, as will be explained in Sections II and IV.

One of the main advantages of Bordé type interferometers is that each of the partial beams and, also important, each of the different exit ports of the Mach-Zehnder interferometer can be labeled by an internal atomic state. This allows one to easily introduce additional state-selective interactions within the interferometer. That the exit ports differ in the internal state allows for a convenient read-out of the interference signal by detecting the number of atoms with a given internal state behind the interferometer. The detection of the exit ports in space is also possible, of course, but it is not necessary and normally rejected in favor of the use of extended and dense atomic samples, increasing the signal to noise ratio by several orders of magnitude, as will be shown in Section IV.

We will discuss examples of highly sensitive measurements of physical quantities with Bordé interferometers in Section V and measurements of topological phase shifts in Section VI. In section VII, quantum measurements with Bordé interferometers will be discussed. Section VIII will concentrate on the application of Bordé interferometers as frequency discriminators for optical frequency standards and atomic clocks.

II. Theoretical Framework

It is often helpful to compare atom interferometers with the well-known optical interferometers. Like an optical interferometer, an atom interferometer consists of beam splitters and zones of free propagation. As such, we can separate the effects of additional interactions that occur in the partial beams from the action of the beam splitters. In the types of interferometers we are going to discuss here, the momentum exchanges connected with the optical excitation of atoms and molecules play the roles of beam splitters and reflectors. The use of laser beams as beam splitters offers a new way of constructing interferometers. Instead of us-

ing beam splitters fixed in space with the atoms traveling through the interferometer, we also can apply a sequence of laser pulses to a spatially extended atomic sample and create an interferometer in the time domain. This pulsed interferometer is of particular importance because the velocity of the atoms can be controlled by laser light. As shown in the following sections, this type of interferometer is even easier to analyze.

The de Broglie wavelength λ_{dB} of the matter wave is given by

$$\lambda_{dB} = \frac{h}{p} \quad (1)$$

where p denotes the atomic momentum and h is Planck's constant. For atoms with thermal energies, this wavelength is on the order of tens of picometers. Because the optical wavelength is large compared with the de Broglie wavelength, the diffraction angle is only a few microradians. This exemplifies the problem one faces in constructing an atom interferometer.

To illustrate the theoretical aspects of atom interferometry, we discuss a particular interferometer, the four-zone Bordé interferometer, with four interactions in the spatial or the temporal domain, as an example of the theoretical description.

A. THE FOUR-BEAM BORDÉ INTERFEROMETER

We treat this interferometer using a simple mechanical interpretation. The interferometer consists of an atomic beam interacting with two counterpropagating pairs of traveling laser beams (Fig. 3). The distance between the co-

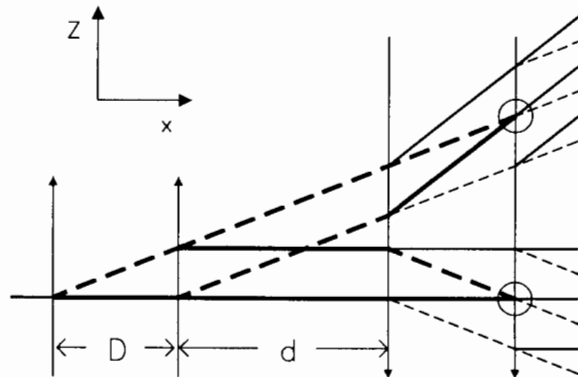


FIG. 3. Four-beam Bordé interferometer, showing all possible atomic paths. The two exit points of the two closed interferometers are indicated by circles.

propagating beams is denoted D , the central distance is d . The beams act as beam splitters, mirrors, and combiners for the atomic wave packets. In each interaction zone, an incoming partial wave is further split into two parts. From the 16 possible partial beams at the output of the interferometer, only the two closed paths indicated in Fig. 3 lead to beams that superimpose coaxially at the output. If we detect an atom behind the fourth interaction zone, we cannot decide which path the atom took and, consequently, we expect interference. The interference pattern for the other paths, not superimposing colinearly, will wash out and not contribute to atom interference. The coherent superposition of the coaxial partial waves at each exit port leads to a periodic variation of the atomic flux with their phase difference. It will be shown in the following text, that this phase difference depends on the frequency of the beam splitter beams. As the different exit ports also differ in their internal states, these interference fringes are usually detected by observing the total flux of excited atoms, such as by detecting their fluorescent decay.

For typical experimental conditions, the separation of these partial beams within the interferometer amounts to tens of micrometers. To increase the signal, usually a much wider atomic beam, with a diameter of about 1 mm is used, with each atom forming its own interferometer. Hence, in this case, the separation of the partial beams is not resolved.

An explanation of the dependency of the fringes on the laser detuning relies on a thorough examination of energy conservation during the interaction of an atom with a single beam splitter, taking into account a detuning between the laser frequency ω_L and the atomic eigenfrequency ω_0 . In this stationary problem of scattering an atom by a light field, energy has to be conserved. For simplicity, we examine the kinematics of two-level atoms with level separation $\hbar\omega_0$. We assume that the atomic beam is propagating along the x axis and the laser beams are propagating along the z direction.

After the excitation into a long-lived state the internal atomic energy is well-defined and equal to $\hbar\omega_0$. The difference between $\hbar\omega_0$ and the photon energy $\hbar\omega_L$ has to be provided by the atomic kinetic energy.

The energy conservation condition is

$$\frac{\mathbf{p}^2}{2m} + \hbar\omega_L = \frac{(\mathbf{p} + \hbar\mathbf{k})^2}{2m} + \hbar\omega_0 \quad (2)$$

This equation gives a condition for the wave vector \mathbf{k} of the absorbed photon:

$$\mathbf{k} \cdot \frac{\mathbf{p}}{m} = \Delta_0 - \frac{\hbar k^2}{2m} \quad (3)$$

with the detuning $\Delta_0 \equiv \omega_L - \omega_0$. Because the beam splitter laser beam is not an infinite plane wave but a localized (Gaussian) beam, its momentum decomposi-

tion contains a range of wave vectors. Equation (3) shows that the atom absorbs a photon from that momentum distribution, which just compensates for the detuning. Depending on the right-hand side of Eq. (3), a component of the absorbed photon momentum \mathbf{k} also will lie along the direction of the atomic beam; that is, in the longitudinal direction. This change in velocity in one partial beam (Sterr *et al.*, 1992) leads to a longitudinal displacement of both partial waves at the exit port by an amount of

$$\Delta x = 2T\hbar(\Delta_0 \pm \delta)/p_z \quad (4)$$

where the plus (minus) sign applies to the lower (upper) interferometer in Fig. 3. The quantity $T \equiv D/v_x$ denotes the time of flight through the distance D and $\delta \equiv \hbar k^2/2m$ denotes the recoil shift of Eq. (3). In addition, as will be shown in the following section, in each excitation–de-excitation process, the phase $\pm\varphi_i$ of the i th laser beam at the location of the interaction is added to the phase of the atomic wave function.

The interference between both partial waves leads to a periodic variation of the excited state population P_e at the output A of the interferometer (Fig. 2):

$$P_e \propto \cos\left(\frac{2\pi\Delta x}{\lambda_{dB}} + \varphi_L\right) = \cos(2T(\Delta_0 \pm \delta) + \varphi_L) \quad (5)$$

where $\varphi_L \equiv \varphi_2 - \varphi_1 + \varphi_4 - \varphi_3$ is the phase introduced by the phases φ_i of the laser beams. This variation of the excited state probability describes the well-known optical Ramsey fringes. Equation (5) assumes an infinite coherence length x_{coh} ; that is, a monochromatic atomic beam with momentum width $\Delta p = 0$. With a finite coherence length $x_{\text{coh}} \equiv \hbar/(2\Delta p)$, fringes are visible only as long as the displacement Δx is smaller than the coherence length. Therefore, with thermal beams, usually only a few fringes are visible.

B. PULSED INTERFEROMETER

In pulsed interferometers (Sengstock *et al.*, 1993a; Kisters *et al.*, 1994), the laser fields that an atom experiences in crossing the spatial sequence of four laser beams is mimicked by a temporal sequence of four laser pulses with separations $T-t-T$ acting simultaneously on all atoms (Fig. 4). Like the four-beam interferometer, the atomic wave function is split and recombined in space by the photon recoil but now with a pulsed experiment; energy conservation (Eq. 2) no longer has to be fulfilled. Instead, the energy uncertainty of the laser pulse (duration τ) provides the energy difference between the average laser frequency $\hbar\omega_L$ and the atomic internal energy. Between the pulses, the atomic wave packet evolves freely with the dynamical phase $\exp(-iEt/\hbar)$ due to its total energy E , which is the sum of the internal energy

($\hbar\omega_0$ for the excited state and 0 for the ground state wave packet) and the kinetic energy

$$E_{\text{kin}} = \frac{(\mathbf{p} + \hbar\mathbf{k})^2}{2m} = \frac{\mathbf{p}^2}{2m} + \frac{\hbar\mathbf{p} \cdot \mathbf{k}}{m} + \frac{\hbar^2\mathbf{k}^2}{2m} \quad \text{and}$$

$$E_{\text{kin}} = \frac{\mathbf{p}^2}{2m} \quad (6)$$

for the excited state and the ground state, respectively. The difference between the kinetic energies leads to a Doppler term proportional to the momentum (which cancels in the third dark period; i.e., between the third pulse and fourth pulse) and the recoil shift. During the laser pulses, the phases of the light field at the time of interaction are imprinted onto the atomic wave functions. At the exit ports the interference between the phases of free propagation and the laser phases leads to a periodic variation of the excited state population P_e of the same form as in the four-beam setup:

$$P_e \propto \cos[2T(\Delta_0 \pm \delta) + \varphi_L]. \quad (7)$$

The atomic wave packets are split and recombined in the direction of the laser beams independent of the laser frequency, and in contrast to the interferometer using an atomic beam, no spatial shift between wave packets is introduced by a

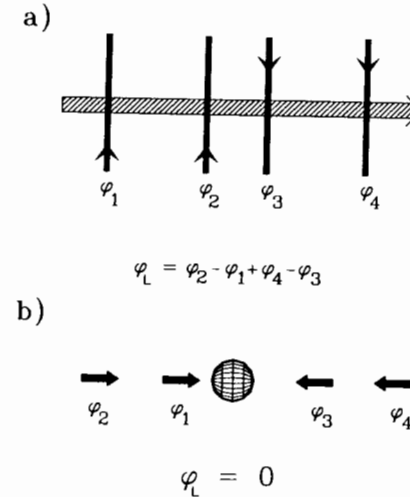


FIG. 4. Scheme for four-zone Bordé interferometry on an atomic beam (a) and a trapped atomic sample (b); for details on the resulting phase φ_L as a sum of laser phases φ_i , see the text.

laser detuning. Consequently, the signal is independent of the atomic coherence length, and the number of visible interference fringes is limited only by the aberrations of the beam splitters (see the following subsection).

C. GENERAL DESCRIPTION

In the following text, we provide a more detailed theoretical description of an atom interferometer in two steps. In the first step (Section II.C.1), we look at the beam splitters in the time and the space domains. The evolution of the atomic wave function between the beam splitters is treated in Section II.C.2. Finally, the influence of additional potentials is discussed in Section II.C.3.

1. Beam Splitters and Combiners

As already mentioned in Section II.A, the laser beams and laser pulses split the atomic wave packets into partial waves with different momenta and different internal atomic states. As in optics, the beam splitters can also be used to combine the partial waves. In the following text, we derive the complex coefficients that describe the probability for the transfer from an input port to an output port. These coefficients are similar to the complex Fresnel coefficients that describe the action of a dielectric beam splitter on optical fields.

We describe the interaction between an atom and a light field by the Schrödinger equation. We assume a two level atom with ground state $|g\rangle$, excited state $|e\rangle$ with optical dipole moment $\boldsymbol{\mu}_e$ and a monochromatic light field $\mathbf{E}(\mathbf{r},t) = \frac{1}{2}\mathbf{E}_0(\mathbf{r},t) \exp(-i\omega_L t) + \text{c.c.}$ with spatially and temporally variable complex amplitude $\mathbf{E}_0(\mathbf{r},t)$.

If the light polarization in all zones is the same, the interaction Hamiltonian H_{int} in the rotating wave approximation (Allen and Eberly, 1975) is given by

$$H_{\text{int}} = \mathbf{E}(\mathbf{r},t) \cdot \boldsymbol{\mu}_e = \frac{1}{2} \hbar \Omega(\mathbf{r},t) \exp(-i\omega_L t) |e\rangle\langle g| + \text{c.c.} \quad (8)$$

Here $\Omega = \mathbf{E}_0 \cdot \boldsymbol{\mu}_e / \hbar$ denotes the (complex valued) Rabi frequency, which determines the coupling of the laser field to the atomic wave due to absorption–stimulated emission. The phase of $\Omega(\mathbf{r},t)$ is the phase of the laser field. In general, the Rabi frequency depends on the atomic position and on time for a pulsed experiment.

The Hamiltonian H_0 for the evolution of the atom contains the internal and kinetic energies:

$$H_0 = \frac{\mathbf{p}_{\text{op}}^2}{2m} + \hbar\omega_0 |e\rangle\langle e| \quad (9)$$

where \mathbf{p}_{op} denotes the momentum operator.

The atomic evolution is governed by the time-dependent Schrödinger equation for the two-component wave function $\Psi = (\langle e|\Psi\rangle, \langle g|\Psi\rangle)^T$ with the Hamiltonian $H = H_0 + H_{\text{int}}$. First we want to treat the interaction with a running wave along the z direction: $E(\mathbf{r},t) = \frac{1}{2} E_0(\mathbf{r},t) \exp(-i\omega_L t + ik_z z) + \text{c.c.}$, with frequency ω_L and wave vector k_z . The field amplitude E_0 characterizes the pulse form and the spatial profile of the laser beam. The Schrödinger equation is

$$i\hbar \frac{\partial}{\partial t} \Psi(\mathbf{r},t) = \left\{ \frac{\mathbf{p}_{\text{op}}^2}{2m} + \frac{\hbar}{2} \begin{bmatrix} 2\omega_0 & \Omega(\mathbf{r},t) \exp(-i\omega_L t + ik_z z) \\ \Omega^*(\mathbf{r},t) \exp(i\omega_L t - ik_z z) & 0 \end{bmatrix} \right\} \Psi(\mathbf{r},t). \quad (10)$$

We can include the excitation energy by going to new basis states, which shift the energies of both states by $\pm\omega_L/2$:

$$\Psi = \begin{bmatrix} \Phi_g(\mathbf{r},t) \exp(-i\omega_L t/2) \\ \Phi_e(\mathbf{r},t) \exp(i\omega_L t/2) \end{bmatrix}. \quad (11)$$

The wave functions Φ_g and Φ_e now give the amplitude of finding the atom at point r in the ground state or excited state. This transformation and the rotating wave approximation simplifies Eq. (10) to

$$i\hbar \frac{\partial}{\partial t} \Phi(\mathbf{r},t) = \left\{ \frac{\mathbf{p}_{\text{op}}^2}{2m} + \frac{\hbar}{2} \begin{bmatrix} -\Delta_0 & \Omega(\mathbf{r},t) \exp(ik_z z) \\ \Omega^*(\mathbf{r},t) \exp(-ik_z z) & \Delta_0 \end{bmatrix} \right\} \Phi(\mathbf{r},t) \quad (12)$$

with detuning $\Delta_0 = \omega_L - \omega_0$. Equation (12) describes the coupling between the two states $|g\rangle$ and $|e\rangle$, differing in momentum by $\hbar k$, in the form of a 2×2 matrix. Because of the complicated dependence of the laser intensity or, equivalently, of the Rabi frequency $\Omega(\mathbf{r},t)$ on time and position, it is not possible to give a general solution to Eq. (12). Luckily, the two cases that are experimentally realized are very well approximated by a purely temporal dependence for the pulsed experiment and by a stationary, but spatially varying, Rabi frequency in the beam experiment.

a. Pulsed Beam Splitters. In the first, conceptually more simple case of the pulsed experiment (see Fig. 4b), the times t_i ($i = 1, 2, 3, 4$) of the interactions are well defined by the experiment. If we neglect the movement of the atoms during

the pulse, the momentum can be treated as a complex number and Eq. (12) simplifies to

$$i\hbar \frac{\partial}{\partial t} \Phi(\mathbf{r}, t) = \frac{\hbar}{2} \begin{bmatrix} -\Delta & \Omega(\mathbf{r}, t) \\ \Omega^*(\mathbf{r}, t) & \Delta \end{bmatrix} \Phi(\mathbf{r}, t) \quad (13)$$

which can be easily integrated to give the well-known Rabi oscillations. Here Δ denotes the Doppler-shifted detuning. Including the first- and second-order Doppler shifts, it is given by

$$\Delta = \Delta_0 - \delta - k \cdot \mathbf{p}/m + \omega_0 v^2/2c^2. \quad (14)$$

In general, an atom in the ground state with momentum p , $|g, \mathbf{p}\rangle$, is transferred during the interaction into a coherent superposition $|\Phi(\mathbf{r})\rangle$ of ground state and excited state, which is given for resonant pulses of length τ and temporal constant Rabi frequency $\Omega(\mathbf{r})$ by

$$|\Phi(\mathbf{r})\rangle = \cos[\Omega(\mathbf{r})\tau/2] |g, \mathbf{p}\rangle - ie^{i\varphi} \sin[\Omega(\mathbf{r})\tau/2] |e, \mathbf{p} + \hbar \mathbf{k}\rangle. \quad (15)$$

Here Ω denotes the absolute value of the Rabi frequency and φ its phase.

In typical experiments, the laser beams for the Ramsey excitation are much wider than the atomic cloud, so that the spatial variation of the laser beam intensity and Rabi frequency in Eq. (15) can be neglected, and the effect of the (resonant) laser pulse is described simply by the 2×2 matrix

$$U = \begin{bmatrix} \cos\left(\frac{\Omega\tau}{2}\right) & -i \sin\left(\frac{\Omega\tau}{2}\right) e^{i\varphi} \\ -i \sin\left(\frac{\Omega\tau}{2}\right) e^{-i\varphi} & \cos\left(\frac{\Omega\tau}{2}\right) \end{bmatrix}. \quad (16)$$

In addition to an intensity-dependent splitting ratio for the outgoing partial waves, one also finds that the phase of the light field is replicated as a phase difference between the exit ports. Note that we have already incorporated the laser frequency ω_L into the definition of the wave function Φ (see Eq. (12)); in the bare states, Ψ , this phase factor would be the total laser phase $\omega_L t_i + \varphi_i$. A 50% beam splitter-combiner is realized with a "pulse area" $\int \Omega(t) dt = \Omega\tau = \pi/2$; that is, with the well-known $\pi/2$ pulse, and a mirror with phase shift φ is realized with a π pulse. The periodic variation of the splitting ratio with the interaction time is analogous to the "pendellösung" of a Bragg interferometer for neutrons or x-rays (see, e.g., Greenberger and Overhauser, 1979).

Important properties of a beam splitter are its chromatic and angular aberrations; that is, its dependence on the atomic momentum. As the interaction time is given by the length τ of the pulse, there is no dependence on the velocity component perpendicular to the direction of the pulsed laser beams (neglecting a sec-

ond-order Doppler effect). A velocity component in the direction of the pulsed laser beams, however, leads to an additional Doppler shift as given in Eq. (14). For laser detunings Δ different from 0, we see from Eq. (13) that the interaction matrix is changed only slightly as long as the detuning Δ is much smaller than the Rabi frequency Ω . In terms of spectroscopy, this corresponds to saturation broadening of the transition. So, in principle, by going to high intensities and short pulses, the beam splitter can be made nearly insensitive to the transverse velocity spread. In many experiments, however, the available laser intensity is not sufficient, limiting the acceptance ranges of the beam splitters to transverse velocities.

It is worthwhile to consider energy conservation in the case of nonzero laser detuning. Even if the laser frequency is not exactly on-resonance, after the pulse we will find some atoms in the excited state. This is no violation of energy conservation, because the pulse of length τ has an energy uncertainty on the order of \hbar/τ .

The situation is more complicated when a pulsed standing wave is used as beam splitter. Now multiple absorption-stimulated-emission cycles from one wave to the other can occur, which can transfer multiple photon momenta. The Hamiltonian now couples an infinite number of momentum states:

$$\begin{aligned} |g, n\rangle &= |g, \mathbf{p} + n\hbar \mathbf{k}\rangle, & n \text{ even, and} \\ |e, n\rangle &= |e, \mathbf{p} + n\hbar \mathbf{k}\rangle, & n \text{ odd.} \end{aligned} \quad (17)$$

This leads to a complicated dependence of the ratio of different orders on the laser frequency, the Rabi frequency, and the angle between \mathbf{p} and \mathbf{k} .

For zero detuning and short pulse length, τ , the laser beam acts like a thin phase grating, and the wave function in the output is given by (Bordé et al., 1984)

$$|\Phi\rangle = \sum_n \left[i^{2n} J_{2n}\left(\frac{\Omega\tau}{2}\right) e^{i2n\varphi} |g, 2n\rangle - i^{2n+1} J_{2n+1}\left(\frac{\Omega\tau}{2}\right) e^{i(2n+1)\varphi} |e, 2n+1\rangle \right] \quad (18)$$

where J_n denotes the Bessel function of order n . The probability for an outgoing partial wave to have acquired $n\hbar k$ of momentum in the z direction is equal to the square of the n th order Bessel function. Because of the many states involved, usually only a few interfere, and the performance of this kind of beam splitter-mirror is not as efficient as the running wave interferometer. The chromatic and angular aberrations are similar to the case of a single running wave.

A different regime for standing-wave light fields is reached when the detuning is much larger than the inverse temporal width of the pulse. In that case, "real" excitation into the excited state is strongly suppressed and all the exiting waves correspond to ground state atoms. This kind of beam splitter is very similar to a mechanical grating beam splitter in the sense that the internal atomic structure plays no important role.

b. Laser Beams as Beam Splitters. The interaction of a moving atom with a cw laser beam is not as easily described. In this case the spatial structure of the beam is essential, and the time invariance of the problem leads to a strict conservation of energy. As a consequence, we can treat the interaction as a scattering between the atom and a laser beam. In this case, we are looking for stationary solutions; that is, with constant energy in the excited state and ground state, separately, which are plane waves in the inward and outward channel with the appropriate momentum in the direction of the laser beams (z direction):

$$|\Phi_{\text{in}}\rangle = \exp(-iEt/\hbar)|g, \mathbf{p}\rangle \quad (19)$$

$$|\Phi_{\text{out}}\rangle = \phi_g \exp(-iEt/\hbar)|g, \mathbf{p}\rangle + \phi_e \exp(-iEt/\hbar + ik_z z)|e, \mathbf{p}\rangle \quad (20)$$

for running waves, and

$$|\Phi_{\text{out}}\rangle = \sum_n \{ \phi_{g,2n} \exp(-iEt/\hbar + 2ink_z z)|g, \mathbf{p}\rangle + \phi_{e,2n+1} \exp[-iEt/\hbar + i(2n+1)k_z z]|e, \mathbf{p}\rangle \} \quad (21)$$

for standing waves, where ϕ denotes the amplitude of the partial wave.

As energy is conserved, we expect that, with a laser detuning different from 0, the energy difference is provided by the center of mass motion. Therefore, in addition to the momentum transfer along the direction of the laser beams, we expect a change in the longitudinal velocity to compensate for the energy difference between photon energy and internal atomic energy, as explained previously.

This longitudinal momentum component stems from the momentum uncertainty of the localized laser beam. If we denote the momentum of the absorbed photon by $\hbar k$, the requirement for energy conservation for an atom leaving the beam splitter in the excited state with a transfer of n photon momenta is

$$\frac{\mathbf{p}^2}{2m} + \hbar\omega_L = \frac{(\mathbf{p} + n\hbar\mathbf{k})^2}{2m} + \hbar\omega_0. \quad (22)$$

This leads, for odd n , that is, for channels with atoms in the excited state, to

$$\frac{n\mathbf{p} \cdot \mathbf{k}}{m} = \omega_L - \omega_0 - \frac{\hbar n^2 \mathbf{k}^2}{2m}. \quad (23)$$

For atomic wave packets leaving the beam splitter in the ground state (even n), the laser detuning does not enter in the energy conservation, and we obtain the Bragg condition:

$$\mathbf{k} \cdot \left(\mathbf{p} + \frac{n\hbar\mathbf{k}}{2} \right) = 0. \quad (24)$$

This means that, as in the case of a running wave, depending on the detuning,

the absorbed photon momentum $\hbar k$ contains a component along the atomic momentum proportional to the detuning for the excited states.

This effect is well known in atomic scattering from a standing wave. Because of the finite size of the interaction, even inside the laser waist, the field is composed of a set of wave vectors with a width $\Delta k = 1/w_0$. For a small waist size w_0 , we observe Kapitza–Dirac scattering; that is, several orders are populated (Gould *et al.*, 1986). For bigger waists (i.e., highly collimated laser beams), energy conservation allows scattering into one order only. This is known as *Bragg scattering* (Martin *et al.*, 1988). The situation is complementary to the pulsed experiments. There, energy was conserved because of the energy–time uncertainty; here, it is because of the position–momentum uncertainty. The use of standing waves as beam splitters was also demonstrated by Giltner *et al.* (1995) and Rasel *et al.* (1995).

To get a quantitative description of the excitation probabilities in a beam experiment with a running wave, we insert the two coupled states of Eq. (20) in Eq. (12). Because of the translational symmetry along the direction of the laser beams (z -direction), the Schrödinger equation separates into a free motion along z for both coupled states and a time-independent Schrödinger equation for the motion perpendicular to the laser beams:

$$E\Phi(x) = \left\{ -\frac{\hbar^2}{2m} \frac{\partial^2}{\partial x^2} - i \frac{p_x \hbar}{m} \frac{\partial}{\partial x} + \frac{p_x^2}{2m} + \frac{\hbar}{2} \begin{bmatrix} -\Delta & \Omega(x) \\ \Omega^*(x) & \Delta \end{bmatrix} \right\} \Phi(x) \quad (25)$$

where Δ is defined in Eq. (14).

If we suppose that we can neglect the second derivative (Raman–Nath approximation), we can introduce a new variable $\xi = mx/p_x$ and end up with

$$i\hbar \frac{\partial}{\partial \xi} \Phi(\xi) = \frac{\hbar}{2} \begin{bmatrix} -\Delta & \Omega(\xi) \\ \Omega^*(\xi) & \Delta \end{bmatrix} \Phi(\xi). \quad (26)$$

This is exactly equivalent to Eq. (13) of the time dependent case, with t replaced by $\xi = x/v_x$.

We now check whether the conditions for the Raman–Nath approximation are justified. We have to compare the value of the first and the second derivatives of Φ with respect to x . From the solution of Eq. (26), we estimate $\partial\Phi/\partial x$ to be on the order Ω/v_x , and $\partial^2\Phi/\partial x^2 \approx \Omega/wv_x$, where w denotes the radius of the laser beam. The second derivative is small if

$$w \gg \hbar/p_x$$

which is very well fulfilled for typical experimental parameters. For example, even for atoms having a momentum p_x equal to the single-photon recoil momentum $\hbar k$, the right side is equal to the optical wavelength, which is typically small compared to the radius of the laser beam. For the phase associated with atomic recoil to be small in the interaction region, one must also require that $w/v_x \ll (\hbar k^2/2m)^{-1}$.

The chromatic aberrations of a beam splitter with laser beams are twofold. First and most important, the interaction time is inversely proportional to the longitudinal atomic velocity. As, to the first order, the excitation probability is periodic in the "pulse area" $\Omega\tau$, a 50% beam splitter ($\Omega\tau = \pi/2$), can be achieved for only a single transverse velocity. On averaging over the velocity distribution of a thermal atomic beam, because of the nonoptimal beam splitter ratios, the maximum averaged contrast of the interferences drops significantly. The aberration due to the transverse velocity is the same as in the pulsed beam splitter.

2. Phases Due to Free Propagation

We will now discuss the free propagation within an atom interferometer. In addition, we are interested in a formalism that allows for easy introduction of additional influences on the atoms during their passage through the interferometer, such as gravitational fields or additional light fields. For the connection between classical physics and quantum mechanics, Feynman's path integral method (Feynman and Hibbs, 1965) provides a convenient way.

Classically, the path Γ_{cl} of the particle in a potential V is determined by the principle of minimum action, $\delta S = 0$ with

$$S = \int_{t_1}^{t_2} L[\mathbf{r}(t), \dot{\mathbf{r}}(t)] dt = \int_{\Gamma_{cl}} \mathbf{p} \cdot d\mathbf{r} - H dt. \quad (27)$$

Here L denotes the Lagrangian $L(\mathbf{r}, \dot{\mathbf{r}}) = \frac{1}{2} m \dot{\mathbf{r}}^2 - V(\mathbf{r})$ and $V(\mathbf{r})$ the potential.

The corresponding quantum mechanical expression was given by Feynman for the transition amplitude $U(\mathbf{r}_1, t_1, \mathbf{r}_2, t_2)$ between two points, \mathbf{r}_1 and \mathbf{r}_2 . The main idea is that, in quantum mechanics, this complex amplitude is determined by all possible paths Γ from \mathbf{r}_1, t_1 to \mathbf{r}_2, t_2 , each contributing a phase S_Γ/\hbar . Usually the phase is very sensitive to the path, so most of the paths interfere destructively. It is only near paths with a stationary phase, that is, near the classical path Γ_{cl} , that many paths can interfere constructively and give a significant contribution to the transition amplitude. For interferometers, with dimensions large compared to the atomic de Broglie wavelength, the quantum mechanical phase is then given by $S_{\Gamma_{cl}}/\hbar$.

In the pulsed interferometer with no additional potentials, the internal energy in the times between the pulses for excited-state atoms is $\hbar\omega_0$ and the Lagrangian for ground and excited-state atoms is

$$L = \frac{mv^2}{2m} \quad \text{and} \quad L = -\hbar\omega_0 + \frac{mv^2}{2m} \quad (28)$$

respectively, where v denotes the actual atomic velocity. Taking into account the

time-dependent transformation of Eq. (11) for the Bordé four-beam interferometer, this reproduces the expression Eq. (5) for the interference signal (Storey and Cohen-Tannoudji, 1994).

In the interferometer using cw laser beams, the same Lagrangian can be applied. The internal energy is the same, but the kinetic energy of the excited state now depends on the detuning, as the energy difference between internal energy and photon energy has to be provided by the atomic kinetic energy. Again, Eq. (5) is reproduced for the example of the four-zone Bordé interferometer. In conclusion, a free propagation is described simply by a phase factor proportional to the difference between internal energy and photon energy.

3. Influence of Additional Potentials

In many applications, the matter-wave interferometer is used to measure phase shifts due to additional potentials that are introduced deliberately into the interferometer.

For small additional potentials, it is possible to start with an ideal interferometer and then treat the potentials as small perturbations. Then, the phase change $\Delta\varphi$ is given by the integral along the unperturbed path, Γ_0 .

In the pulsed experiment, if the additional potential is spatially constant and varies only in time, the path remains the same and the only change in the integrand comes from the change in the potential V :

$$\Delta\varphi = -\frac{1}{\hbar} \oint_{\Gamma_0} V(t) dt. \quad (29)$$

For an atomic beam with cw excitation zones, the total energy remains constant, so the only phase change is due to the change in the momentum

$$\Delta\varphi = \frac{1}{\hbar} \oint_{\Gamma_0} \Delta\mathbf{p} \cdot d\mathbf{r}. \quad (30)$$

A semi-classical wave function that takes into account the phase S_Γ/\hbar for conditions where the change of the wave function over one de Broglie wavelength is small is given by the WKB wave function

$$\Psi(\mathbf{r}, t) \propto \exp \left[\frac{i}{\hbar} \int_{r_0}^r (p dr - E dt) \right] \quad (31)$$

where the momentum p is the classical momentum at a constant energy:

$$p = \sqrt{2m[E - V(r)]}. \quad (32)$$

The phase term of Eq. (31) is also known as the *eikonal*.

For weak potentials $V \ll E$, this expression can be expanded, and the phase shift (Eq. 30) introduced by the potential is

$$\Delta\varphi = \int \Delta p/\hbar dx = -\frac{1}{\hbar v} \int V(r) dr. \quad (33)$$

A special class of potentials arises from potentials connected with inertial forces like accelerations, gravitation, or rotations. These are not localized to an interaction zone well between the beam splitters but affect the whole interferometer. The classical paths in larger additional potentials do not completely overlap, so wave fronts originating from different source points interfere. This is similar to an optical shearing interferometer. In this case, the interference pattern is determined by the coherence properties of the source. For a deeper discussion with respect to a neutron interferometer, see Greenberger and Overhauser (1979).

In the next section we will present an overview of different types of interferometers using lasers as beam splitters, where we will briefly discuss the influence of various potentials.

III. Discussion of Different Types of Interferometers

Now that we have presented all the building blocks, we have to combine them to form a working interferometer. As in optics, it is not enough to split and recombine the wave. The interferometer also has to be designed to work with the given coherence length of the source; that is, to combine waves from the same coherence volume. In an interferometer using thermal atoms, these issues are even more difficult because of the small wavelength and the short coherence length. In the case of matter-wave interferometers with lasers as beam splitters, the dependence of the interference fringes on the laser frequency and the aberrations of the beam splitter (e.g., Doppler shift) also have to be considered.

A very convenient way to visualize the interferometer is by drawing the classical paths within the interferometer. Important characteristics can be read from these diagrams. Because of its experimental simplicity, usually the integral flux in the excited state or ground state in all output beams is measured. In this case, only interference from partial waves with atoms in the same internal state can be observed.

To obtain interference patterns in the integral flux, the phase shift has to be constant across the width of the atomic beam. Therefore, the exit paths have to be parallel to an angle α better than $\alpha < \lambda_{\text{dB}}/2r$, where $2r$ is the diameter of the atomic beam. Otherwise, spatial interference fringes, such as those observed in optical interferometers, appear that will wash out any interference when averaged over the size of the atomic beam. Because of the small atomic de Broglie wavelength, this is a very stringent condition. In interferometers based on sepa-